A&A, 709, A92 (2026)
https://doi.org/10.1051/0004-6361/202659250

Astronomy & Astrophysics

Where within the 3C 84 jet are γ-rays produced?

Georgios F. Paraschos[1,2,3,⋆], Ioannis Liodakis[4,3], Svetlana Jorstad[5,6], Yuri Y. Kovalev[3], Sudip Chakraborty[7], Frédéric Marin[8], Steven R. Ehlert[7], Efthalia Traianou[8,3], Lena C. Debbrecht[3], Iván Agudo[10], Thibault Barnouin[8], Jacob J. Casey[11], Laura Di Gesu[12], Philip Kaaret[7], Dawoon E. Kim[13], Fabian Kislat[11], Ajay Ratheesh[14,13], M. Lynne Saade[15,7], Francesco Tombesi[16,17], Alan Marscher[5], José-Luis Gómez[10], Alexander B. Pushkarev[18,19,20], Tuomas Savolainen[21,2,3], Ioannis Myserlis[22], Mark Gurwell[23], Garrett Keating[23], Ramprasad Rao[23], Sincheol Kang[24], Sang-Sung Lee[24,25], Sanghyun Kim[24], Whee Yeon Cheong[24], Hyeon-Woo Jeong[24,25], Chanwoo Song[24,25], Shan Li[24,25], Myeong-Seok Nam[24,25], Diego Álvarez-Ortega[4,26], Carolina Casadio[4,26], Chien-Ting Chen[15], Enrico Costa[13], Eugene Churazov[27], Riccardo Ferrazzoli[13], Giorgio Galanti[28], Ildar Khabibullin[29,27], Stephen L. O'Dell[7], Luigi Pacciani[13], Marco Roncadelli[30], Oliver J. Roberts[15], Paolo Soffitta[13], Douglas A. Swartz[15], Fabrizio Tavecchio[31], Martin C. Weisskopf[7], and Irina Zhuravleva[32]

(Affiliations can be found after the references)

Received 31 January 2026 / Accepted 19 March 2026

ABSTRACT

The location in which γ-ray are created and emitted within extra-galactic jets is a matter of active debate. One particularly well-suited source for determining the location is the nearby bright radio galaxy 3C 84, harbouring a powerful jet. We investigated the origin of γ-rays that were measured during a recent γ-ray flare by analysing the linear polarisation signal of close-in-time very long baseline interferometry (VLBI) observations at centimetre and millimetre wavelengths. While 3C 84 is almost unpolarised overall, we find that close in time to the γ-ray flare peak regions at parsec-scale distances from the central engine, the linear polarisation increases fractionally. Under the physically well-motivated assumption of a causal relation between this polarisation enhancement and the γ-ray flare, and combined with insights from concurrent X-ray polarisation measurements, a physically motivated scenario is that the γ-rays are created in this region, in a process consistent with the synchrotron self-Compton mechanism.

Key words. techniques: high angular resolution – techniques: interferometric – techniques: polarimetric – galaxies: active – galaxies: individual: 3C 84 – galaxies: jets

1. Introduction

Flares that are bright in γ-rays are a common feature in the light curves of astrophysical jets. It is thought that such flares are a direct result of the highly energetic plasma beam powered by a central supermassive black hole (SMBH) inside an active galactic nucleus (AGN) that interacts with itself and its environment (see e.g. MacDonald et al. 2017; Lico et al. 2017). However, questions still remain about the exact location of their origin within the entirety of the jet. Trying to answer these questions requires investigating powerful nearby jets, for which we can use the resolving ability of centimetre and millimetre very long baseline interferometry (VLBI) to directly probe the possible emission regions with high fidelity.

For the work presented here, we chose the nearby radio galaxy 3C 84 (NGC 1275; $z = 0.0176$, Strauss et al. 1992), which harbours a powerful radio jet and also recently exhibited a bright γ-ray flare. While 3C 84 has been studied for many decades (e.g. Backer et al. 1987; Krichbaum et al. 1992; Homan & Wardle 2004; Nagai et al. 2010; Paraschos et al. 2022) in which the source fluctuated between periods of intense activity and comparative quiescence, it is still unclear where the γ-ray location lies. Attempts have been made in the past to determine the exact location by means of a variability light-curve correlation and by investigating structural changes within the jet. For example, works by Hodgson et al. (2018), Hodgson et al. (2021), Paraschos et al. (2023), Sinitsyna & Sinitsyna (2025) came to the conclusion that the long-term variability is consistent with multiple emission regions from near the jet origin and from farther downstream in the parsec-scale region. Furthermore, works by Abdo et al. (2009) and Nagai et al. (2010), which investigated the connection between a radio and γ-ray flare in 2008, favoured a downstream emission region.

We explore the connection between a recent γ-ray flare reported in 3C 84 and the concurrent change in linear polarisation within the jet. This work was motivated by the multi-wavelength campaign that was initiated by the Imaging X-ray Polarimetry Explorer (IXPE; Weisskopf et al. 2022; Soffitta et al. 2023), with an observing time of the source between January and March of 2025. These observations are the longest ever IXPE observations of a source to date, lasting 2.5 Msec (see Liodakis et al. 2025, for details). 3C 84 is known to exhibit an ordered magnetic field associated with its jet (see Paraschos et al. 2024a,b), and an increase in linear polarisation is a signature that the magnetic field is enhanced (see also MacDonald & Nishikawa 2021; Kramer et al. 2024). This can be connected to flaring activity. We note, however, that 3C 84 generally exhibits low linear polarisation, of about 1% at

⋆ Corresponding author: gfpara@utu.fi

Table 1. VLBI epochs.

BEAM-ME (43 GHz)					MOJAVE (15 GHz)		
Date	I_{Core} [Jy]	PD_{Core}	I_{C3} [Jy]	PD_{C3} [%]	Date	I_{tot} [Jy]	PD_{tot} [%]
04 Apr. 2025	6.7 ± 0.7	<0.7	0.7 ± 0.1	7 ± 2.1	16 Mar. 2025	32.7 ± 1.6	∼0.1
23 Mar. 2025	8.5 ± 0.9	1.1 ± 0.2	0.9 ± 0.1	7 ± 1.7	21 Feb. 2025	45.4 ± 2.3	<0.1
09 Mar. 2025	8.3 ± 0.8	1.3 ± 0.2	0.7 ± 0.1	<7.7	26 Jan. 2025	40.7 ± 2.0	∼0.1
16 Feb. 2025	7.7 ± 0.8	1.2 ± 0.2	0.8 ± 0.1	9 ± 2.0	06 Jan. 2025	45.1 ± 2.3	∼0.1
15 Dec. 2024	8.6 ± 0.9	1.2 ± 0.2	1.1 ± 0.1	12 ± 1.8	26 Nov. 2024	42.5 ± 2.1	<0.1
21 Nov. 2024	10.0 ± 1.0	1.0 ± 0.2	1.0 ± 0.1	5 ± 1.4			

Notes. The left part of the table corresponds to the 43 GHz BEAM-ME observations, and the right part shows the 15 GHz MOJAVE (`CLEAN`-reconstructed) observations. From left to right, the columns indicate the observation date, the total intensity of the area of interest (core and C3 for the 43 GHz observations, total for the 15 GHz ones), and the linear polarisation degree. They were calculated by integrating the flux density within an area the size of the nominal `CLEAN` beam.

43 GHz, but this increases with frequency (see, e.g. Nagai et al. 2017; Kim et al. 2019). We report an enhancement of the linear polarisation at a distance of ∼1.5 parsec[1] from the central engine (Paraschos et al. 2021) during the 2025 γ-ray flare. In Sect. 2 we present the observations and our results, which we discuss in Sect. 3. Finally, we summarise our work in Sect. 4.

2. Methods

2.1. Observations

3C 84 was observed in VLBI mode at 15 GHz and 43 GHz; specifically, the 15 GHz Very Long Baseline Array (VLBA) sessions were observed as part of the Monitoring of Jets in Active galactic nuclei with VLBA Experiments (MOJAVE) programme (Lister et al. 2018)[2], and the 43 GHz VLBA sessions were conducted as part of the Blazars Entering the Astrophysical Multi-Messenger Era (BEAM-ME) programme (Jorstad & Marscher 2016)[3]. The epochs we used are presented in Table 1. Furthermore, 3C 84 was observed in single-dish and connected interferometer (s.d./c.i) mode between 22 GHz and 225 GHz. These observations were conducted between mid January 2025 and the beginning of April 2025 (see Fig. 1). The participating telescopes were the Korean VLBI Network (KVN; Kang et al. 2015, observing at 22, 43, 86, and 129 GHz), the IRAM-30 m telescope (via the Polarimetric Monitoring of AGN at Millimeter Wavelengths programme Agudo et al. 2018, observing at 86 and 225 GHz), and the Submillimeter Array (SMA; via the SMA Monitoring of AGNs with Polarization; see Myserlis et al. in prep.). The relevant details are discussed in Liodakis et al. (2025).

In a fortunate turn of events, Monti-Guarnieri & Bernard (2025) reported enhanced γ-ray emission from a location consistent with 3C 84 as detected with the *Fermi* Large Area Telescope (LAT; Abdollahi et al. 2023) in early January 2025, with activity spanning between December 2024 and March 2025. These γ-ray observations, pulled directly from the publicly available repository[4], binned in three-day intervals using a free spectral index, are also presented in Fig. 1. As this time frame coincides with our VLBI measurements, we were able to investigate the changes in the jet before, during, and after this flare.

2.2. Data analysis

We used all available epochs during the time frame of interest from the MOJAVE and BEAM-ME monitoring programmes, which provide publicly available calibrated VLBI data (see Jorstad et al. 2017; Lister et al. 2018, for a description of the calibration and imaging procedures). We re-imaged the BEAM-ME data using the regularised maximum likelihood (RML) method implemented in the software suite `eht-imaging` (Chael et al. 2016, 2018), and we used the MOJAVE data as they are provided by the MOJAVE collaboration, without reanalysis. Given the high brightness of 3C 84 at 43 GHz, we achieved high-resolution imaging that recovered detailed total intensity and polarimetric structure. Unlike traditional `CLEAN`-based approaches, RML uses forward-modelling with physically motivated regularisers, such as total variation, entropy, and sparsity, to manage sparse VLBI coverage while preserving fine-scale structure (Event Horizon Telescope Collaboration 2019, 2022). This approach is particularly well suited for complex sources such as 3C 84 that are characterised by filamentary structures, for which a geometrical model fitting may be less reliable (see, e.g. Paraschos et al. 2024c, for an implementation on core-jet morphologies). Furthermore, the possibility of super-resolution compared to `CLEAN` that RML offers facilitates the exact spatial determination of the polarised emission.

In order to determine the regularisation terms needed to fit all datasets best, we varied them across a search grid after accounting for non-closing systematic errors of 1% of the visibility amplitude (see Traianou et al. 2025, for more details on the procedure, which involves solving for both complex visibilities and closure quantities, and the regularisation terms). These terms include the $\ell 1$ norm, the relative entropy mem, the total variation tv, the total squared variation tv2, and the total variation $\ell 2$ with the logarithmic regularising term tv2log. The set of regularisation terms fitting all epochs best ($\chi^2 \approx 1$) were $\ell 1 = 0.6$, mem = 0.1, tv = 0, tv2 = 1.3, and tv2log = 0.02 for the corresponding data terms $\alpha_{amp} = 50$, $\alpha_{cp} = 90$, and $\alpha_{lca} = 90$ (see also Janssen et al. 2021).

On the other hand, while the 15 GHz observations offer a higher sensitivity, the source is known to exhibit a decreasing linear polarisation flux density trend with decreasing frequency. Therefore, we did not expect effective data for our present analysis, as also shown in Sect. 2. As a sanity check, we also

[1] For our work we assume a Λ cold dark matter cosmology (ΛCDM) model, with $H_0 = 67.8\,\mathrm{km\,s^{-1}\,Mpc^{-1}}$, $\Omega_\Lambda = 0.692$, and $\Omega_M = 0.308$ (Planck Collaboration XIII 2016), which results in a megaparsec luminosity distance of $D_L = 78.9 \pm 2.4$ Mpc and a parsec-to-milliarcsecond (pc-mas) conversion factor of $\psi = 0.36\,\mathrm{pc\,mas^{-1}}$.

[2] https://www.cv.nrao.edu/MOJAVE/index.html

[3] https://www.bu.edu/blazars/BEAM-ME.html

[4] https://fermi.gsfc.nasa.gov/ssc/data/access/lat/LightCurveRepository/

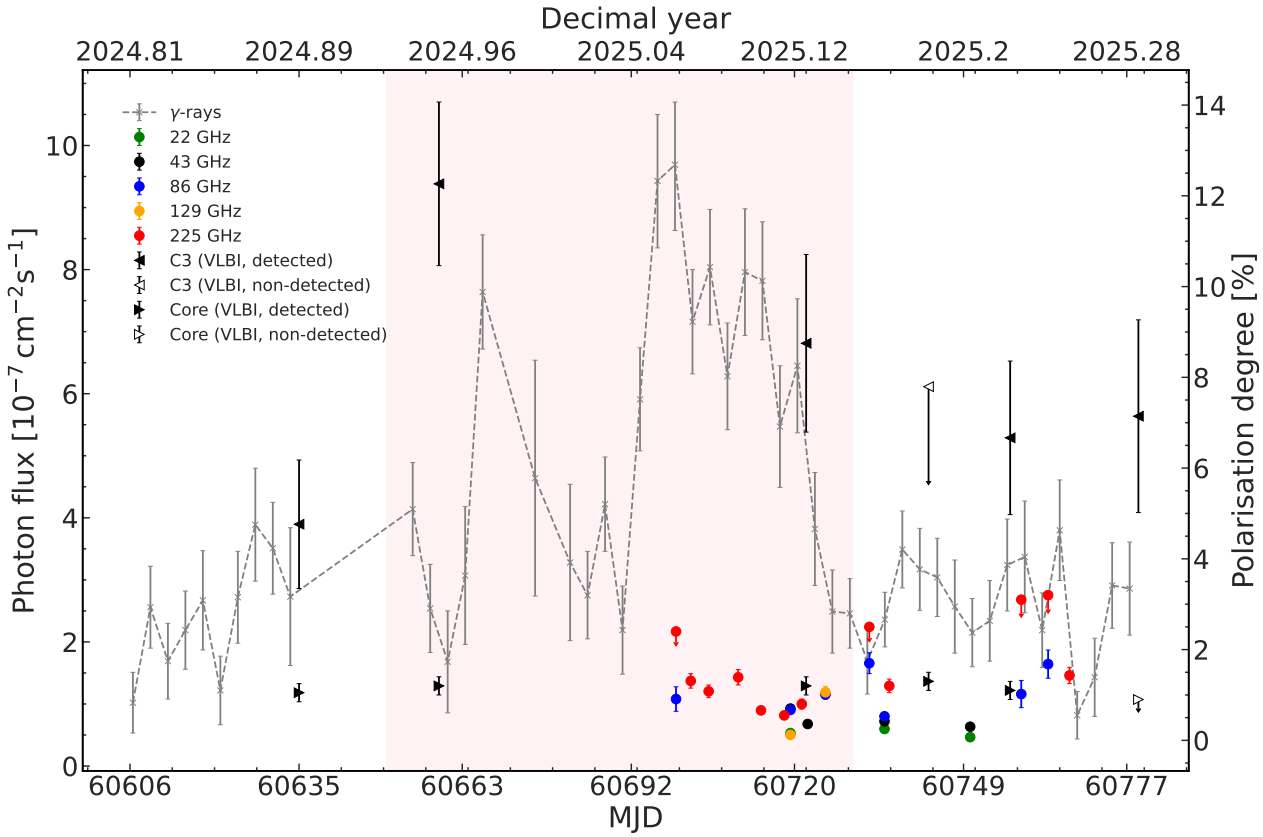

Fig. 1. Linear polarisation degree and γ-ray flux as a function of time. We show observations taken with the KVN at 22, 43, 86, and 129 GHz, with the IRAM 30 m telescope as part of the POLAMI programme at 86 and 225 GHz, with the SMA at 225 GHz (all in colour and circles) and Fermi-LAT in γ-rays (grey crosses connected by a dashed line). In addition, the black triangles denote the VLBI polarisation degree of the core and C3 at 43 GHz. The filled triangles with an error bar correspond to a detection (close to the γ-ray peak, with the entirety of the flare being denoted with the shaded light pink area), the empty triangle to a non-detection upper limit. All values are listed in Table 1. The well-known trend for 3C 84 of higher polarisation values at higher frequencies is observed here as well. The radio observation dates span from MJD 60696 to 60767. During this time frame, some depolarisation is also observed, possibly because multiple jet components blurred the s.d./c.i measurements.

compared our results with the publicly available `CLEAN` images of BEAM-ME. By employing both reconstruction methods, performed by different teams (because the publicly available nature of the 43 GHz data was analysed independently by the BEAM-ME team), we achieved added robustness to our results. The overall jet structure (although resolved in more detail in our approach) and flux densities agree well (see also Fig. A.1).

Importantly for this work, `eht-imaging` simultaneously reconstructs Stokes Q and U during polarimetric imaging by applying constraints such as the Holdaway-Wardle limit and polarimetric total variation to ensure physical consistency (Holdaway & Wardle 1990; Event Horizon Telescope Collaboration 2021; Traianou et al. 2025). The integration of the instrumental calibration within the imaging loop further improves convergence and image fidelity, making the method well suited to low-polarisation sources like 3C 84 (Event Horizon Telescope Collaboration 2021).

2.3. Results

We present the results of our millimetre VLBI analysis, shown in Fig. 2 (top panel), and we also discuss them below (our centimetre VLBI analysis, exhibiting a lower overall linear polarisation signal consistent with the source history is shown in the bottom panel; total intensity images are available online). For both frequencies the images are aligned at the so-called radio core. Defining and identifying the core in a VLBI image is a delicate matter and is subject to a number of assumptions. In our case, we followed the vast number of publications available for 3C 84 over the years (see, e.g. Lister et al. 2018; Weaver et al. 2022, for two recent examples of VLBI monitoring of the source at cm VLBI wavelengths over decades), which placed the centimetre VLBI core at the brightest area inside the northernmost part of the jet. 3C 84 is characterised by a low total integrated polarisation overall that is ∼1%. In the core, we detected linear polarisation in most epochs (see Table 1). However, during the γ-ray flare peak (at the December 15, 2024, epoch) the fractional linear polarisation was enhanced in regions downstream of the central engine. Therefore, we focus on the region downstream of the core in the remainder of this work. Specifically, the area 1.5 parsec away from it (denoted C3), identified with the jet termination region (Kam et al. 2024), exhibits a brightening in the linear polarisation. The respective values are listed in Table 1. We point out here that the calibration uncertainty of the linear polarisation (commonly referred to as D-term calibration) is about 0.9%, indicating that our detections are robust. This value was calculated by averaging the D-term corrections of all sources of the epochs in question, as calculated using the procedure described in Jorstad et al. (2017), because we did not recalibrate the already calibrated D-terms in our imaging procedure.

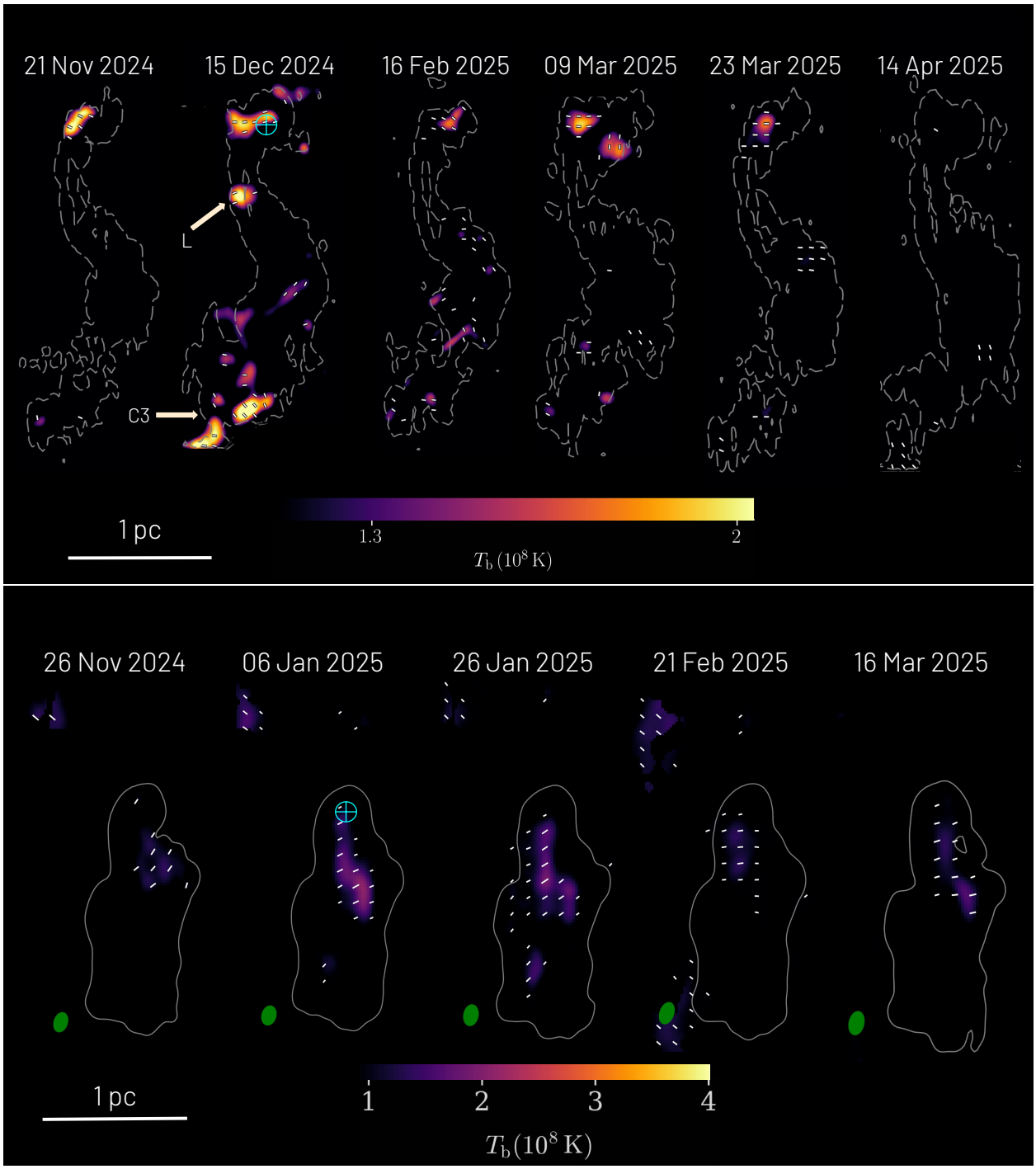

Fig. 2. Images of 3C 84 at 43 GHz (BEAM-ME) and 15 GHz (MOJAVE). *Top panel*: 43 GHz total intensity (contours) and linear polarisation (colour) images of 3C 84 for all available epochs during the time frame of interest. The contour levels were set at 1% of the total intensity maximum (I_{max}) per epoch. The linear polarisation flux density is displayed in units of brightness temperature. The chosen colour scale is meant to display the detections while also masking the surrounding noise. The cyan cross and circle denote the core region and the arrows show C3, as discussed in the main text, and region L (see discussion in Sect. 3). The white sticks indicate the EVPAs. At the epoch nearest to the γ-ray flare peak (15 Dec. 2024), we detect linear polarisation at a distance of ∼1.5 parsec (C3) from the central engine. *Bottom panel*: 15 GHz images of the 3C 84 jet for the available epochs in the time frame of interest, shown in a similar manner as in the top panel, prepared by the MOJAVE collaboration (CLEAN-reconstruction). The green ellipse next to each reconstruction illustrates the restoring CLEAN-beam, which corresponds to (0.8×0.5) mas (15°) on average. We note that the linear polarisation is similar in magnitude to the noise level, amounting to marginal detections.

Furthermore, we note that a region (denoted L in Fig. 2) that is also outside the compact core, at a distance of ∼0.5 parsec, exhibits a brightness increase as well, but only in the December 15, 2024, epoch. For the MOJAVE measurements, we found that the linear polarisation signal is weaker, as is consistent with the historical linear polarisation values of 3C 84.

As shown in Fig. 1, the VLBI polarisation degree exhibits higher values at the onset of the γ-ray flare overall and then decreases in the aftermath (see also Fig. B.1 for the behaviour

Table 2. Linear polarisation measurements of 3C 84 in s.d./c.i mode.

Frequency [GHz]	MJD	Polarisation degree [%]	Position Angle [deg]
22*	60719.3	0.16 ± 0.01	−4.33 ± 12.33
22*	60735.4	0.25 ± 0.03	16.92 ± 9.35
22*	60750.1	0.07 ± 0.04	18.47 ± 1.74
43*	60719.3	0.70 ± 0.03	112.20 ± 1.45
43*	60722.3	0.36 ± 0.04	124.38 ± 3.83
43*	60735.4	0.42 ± 0.03	105.07 ± 3.89
43*	60750.1	0.30 ± 0.06	134.19 ± 5.24
86†	60699.7	0.91 ± 0.27	51.5 ± 7.0
86*	60722.3	0.67 ± 0.10	76.60 ± 3.20
86*	60725.3	1.01 ± 0.10	49.93 ± 3.59
86†	60732.8	1.70 ± 0.23	23.6 ± 3.8
86*	60735.4	0.53 ± 0.07	63.59 ± 4.51
86†	60758.9	1.02 ± 0.30	24.8 ± 7.7
86†	60763.5	1.68 ± 0.31	54.8 ± 4.6
129*	60719.3	0.12 ± 0.08	63.46 ± 2.73
129*	60725.3	1.06 ± 0.13	31.28 ± 4.25
225†	60699.7	<2.4	–
225□	60702.2	1.31 ± 0.16	−28.80 ± 1.85
225□	60705.3	1.08 ± 0.14	−15.72 ± 1.92
225□	60710.3	1.39 ± 0.17	−26.21 ± 1.98
225□	60714.3	0.66 ± 0.09	−11.25 ± 1.45
225□	60718.2	0.55 ± 0.08	−7.07 ± 1.01
225□	60721.3	0.80 ± 0.11	−11.29 ± 1.46
225†	60732.8	<2.5	–
225□	60736.3	1.20 ± 0.15	23.00 ± 2.04
225†	60758.9	<3.1	–
225□	60767.2	1.43 ± 0.18	17.74 ± 1.92
225†	60763.5	<3.2	–

Notes. *KVN; †POLAMI; □SMA.

of the total intensity). While the uncertainties are large, a clear trend exists that suggests that this rise during the γ-ray flare is real. A χ^2 test against the hypothesis of a constant polarisation degree (in essence, a model in which the ratio of the Stokes I and the linear polarisation P remains constant per measurement and any deviation is attributed to measurement noise) yields $\chi^2 = 14.5$ for four degrees of freedom ($\chi^2_{\rm red} = 2.89$, $p = 0.01$), indicating statistically significant variability during the observing window. The s.d./c.i polarisation degree measurements indicate an enhancement after the γ-ray flare peak before it dims again. The measurements also follow the trend of a higher linear polarisation at higher frequencies. We note that the apparent depolarisation might be connected to the fact that the s.d./c.i observations capture the entirety of the jet, which can have a smearing effect because different regions are probed that contribute to the measurements. The electric vector position angles (EVPAs; see Table 2) at 22 and 225 GHz appear to be aligned with the north-south jet direction, whereas the other frequencies seem to diverge.

3. Discussion

Locating the exact position of γ-ray production within jets has been a topic of active research in recent years, and nearby jetted radio galaxies offer a unique laboratory for directly examining the possible locations. 3C 84 is such a jet, whose morphology has carefully been monitored over the years. Its parsec-scale jet consists of three characteristic regions, referred to as C1 (core), C2 (diffuse parsec-scale region), and C3 (bright moving knot). They are connected by a double-rail structure and are surrounded by a cocoon (Savolainen et al. 2023). This filamentary structure, which reaches deep into the core region (Nagai et al. 2014; Giovannini et al. 2018) and indicates transverse jet stratification, has been interpreted as a possible manifestation of a Kelvin-Helmholtz instability (Paraschos & Mpisketzis 2025).

In this complex structure, it is hard to determine the exact location of the γ-ray emission zone. It is particularly important to find this location because it is thought to coincide with the elusive blazar zone (Hovatta & Lindfors 2019), in which particles are accelerated to the high energies we commonly observe in blazar jets. Two scenarios are usually invoked: the near site (within the broad line region which provides the photon field for upscattering, see Sikora et al. 1994; Blandford & Levinson 1995, among others) and the far site (beyond the broad line region, e.g. Lähteenmäki & Valtaoja 2003; Lindfors et al. 2006; Marscher et al. 2012; Jorstad et al. 2013; Kramarenko et al. 2022). Previous studies, which have tried to determine the location of γ-ray emission within the 3C 84 jet (e.g. Hodgson et al. 2018, 2021; Paraschos et al. 2023; Sinitsyna & Sinitsyna 2025) by investigating the long-term behaviour of the multi-band light curves of the source, have provided evidence in favour of both scenarios.

We found indications that γ-rays emitted during the recent flare in early 2025 originated far from the central engine, at a distance of ∼1 parsec. We based this assessment on our linear polarisation analysis, which revealed a brightness

enhancement in this region, which is a signature of an ordered increase in the magnetic field amplitude. Under the assumption that the linear polarisation enhancement is associated with the γ-ray flare, our result suggests that 3C 84 has likely been producing γ-rays downstream of the central engine for at least the last two decades (Abdo et al. 2009; Nagai et al. 2010). This assumption is well motivated because similar behaviour has been explained theoretically (e.g. Hughes et al. 2011) and was also noted for a number of sources in the literature, for example, OJ 287 (Agudo et al. 2011), 3C 279 (Rani et al. 2017), 3C 454.3 (Liodakis et al. 2020), OJ 248 (Paraschos 2025), PKS 0735+178 (Paraschos et al. 2025), and 3C 120 (Traianou et al. 2026). While the examples above do not disprove a chance coincidence of a radio polarisation degree enhancement alongside a γ-ray flare, they do indicate that a causal connection is plausible. Nevertheless, in these cases, a transient increase in the fractional linear polarisation signals a shock- or reconnection-driven ordering and compression of the magnetic field. The ordered field increases the synchrotron emissivity and the local synchrotron photon energy density, which in turn produces the observed γ-ray flare (possibly through synchrotron self-Compton emission, as also discussed further below). We note that the brightness enhancement in region L only appears in the December 15, 2024, epoch; its absence from all other epochs, along with it being rather compact and localised, indicates that it might be an imaging artefact caused by the low signal to noise ratio in this area. Stacking the total intensity and polarised BU images used here in time did not reveal any pronounced activity in this region. If, however, this region is not an artefact, then it is at a distance of ∼1 parsec to C3, indicating that the region and C3 are most likely not causally connected; instead, multiple emission regions, such as those created by multiple shocks, turbulence, or magnetic reconnection, for example by jet-in-jet models, appear to be more likely (see e.g. Giannios et al. 2009; Narayan & Piran 2012; Clausen-Brown & Lyutikov 2012; Biteau & Giebels 2012; Dotson et al. 2015).

Furthermore, the IXPE study by Liodakis et al. (2025) that accompanies our study here revealed that the X-ray position angle is parallel to bulk jet flow and that the X-ray polarisation is about 4%. The authors also showed that optical and γ-ray variability is strongly correlated at a time lag consistent with zero days, with the optical photons originating mainly from synchrotron emission as a precursor of synchrotron self-Comptonised X-ray and γ-ray photons (Marin et al. 2025). The authors interpreted their results as being caused by the synchrotron self-Compton emission mechanism.

Motivated by these findings, we designed our analysis to address the plausibility of SSC in our case. Our approach was twofold: we first performed a comparative analysis to ascertain whether the physical conditions present in the C3 region of 3C 84 are able to cause the observed γ-ray flare, whose peak value was about $F_{\rm SSC}^{Fermi} \sim 4\times10^{-4}\,{\rm MeV/cm^2/s}$. Assuming equipartition between the particle and magnetic energy, we started by estimating the magnetic field strength in the emitting region from the synchrotron self-absorption (SSA) turnover parameters following the procedure outlined in Appendix D of Paraschos et al. (2024b), based on the formalism of Marscher (1983). For a homogeneous spherical synchrotron source with an angular diameter $\theta_{\rm mas}$ and a turnover frequency ν_m [GHz] at which the observed flux density is S'_m [Jy], the SSA magnetic field in Gauss is given by

$$B_{\rm SSA} = 10^{-5}\, b(\alpha)\, \theta_{\rm mas}^{4}\, \nu_m^{5}\, S'^{-2}_{m}\, \frac{\delta}{1+z}\,[{\rm G}], \quad (1)$$

where $b(\alpha)$ is a dimensionless function tabulated by Marscher (1983) that depends on the optically thin spectral index α ($S_\nu \propto \nu^\alpha$), δ is the Doppler factor, and z is the source redshift. We adopted $\alpha = -0.5$, for which $b(\alpha) \simeq 3.2$, set $\delta = \delta_{\rm eq} = 1.5$ (Paraschos et al. 2024b), and estimated the emitting region size from our current data to be $\theta_{\rm mas} \sim 0.15$ mas (including the correction factor discussed in Marscher 1983), based on the size reported by Lister et al. (2019), Paraschos et al. (2022), and Kam et al. (2024), and we then logarithmically interpolated this to the turnover frequency (see Pushkarev et al. 2019, for more details). For the turnover parameters, Kim et al. (2019) and Paraschos et al. (2024b) placed the turnover frequency and turnover flux in the ranges $\nu_m = 86{-}113$ GHz and $S'_m = 5.6{-}9.0$ Jy in the core region. Lower values of about $\nu_m \sim 20$ GHz (e.g. Benke et al. 2026) are expected downstream in a quiescent state. In a flaring state, however, as is our case, the turnover parameters are expected to rise again, as shown by Valtaoja et al. (1992), Fromm et al. (2016), and Fuhrmann et al. (2016). Furthermore, we computed the spectral indices α in the C3 area for the three epochs closest to the flare (i.e. the first three epochs of each frequency in Fig. 2), following the procedure described in Paraschos et al. (2021). The different frequency images used for the spectral analysis were not taken quasi-simultaneously, but 3C 84 is known to not vary over a fortnight (e.g. Paraschos et al. 2022; Park et al. 2024). We found that before and after the flare, $\alpha \sim -0.80$, while during the flare, $\alpha \sim 0.35$, indicating higher turnover frequency values. This spectral index trend is similar to the polarisation trend shown in Fig. 1. We note that the uncertainties are about 0.2, which can substantially affect the final turnover frequency values. Finally, we calculated the flux density at the turnover frequency $\nu_m = 60$ GHz via the standard formula $S \propto \nu^\alpha$, using the measured 43 GHz total intensity flux density of C3 during the flare (see Table 1). Under these conditions, $B_{\rm SSA} \sim 3.0$ G.

Then, continuing with the formalism presented in Marscher (1983), the synchrotron self-Compton flux density can be approximated by the following equation:

$$F_{\rm SSC}(E_{\rm keV}) = d(\alpha)\ln\left(\frac{\nu_2}{\nu_m}\right)\theta_{\rm mas}^{-2(2\alpha+3)}\nu_m^{-(3\alpha+5)}S'^{2(\alpha+2)}_{m} E_{\rm keV}^{-\alpha}\left(\frac{1+z}{\delta}\right)^{2(\alpha+2)}\,[\mu{\rm Jy}]. \quad (2)$$

Here, $d(\alpha)$ is another dimensionless function, $\nu_2 \equiv 2.8\times10^6 B_{\rm SSA}\gamma_2^2$ is the frequency cut-off to the synchrotron spectrum, with $\gamma_2^2 = 5\times10^5$ (we used a characteristic value from the range reported in Abdo et al. 2009), and $E_{\rm keV}$ is the photon energy in the observer's frame (we assumed a typical value of 10^6 keV for a TeV source such as 3C 84). Plugging in all the aforementioned values yielded $F_{\rm SSC} \sim 0.4\times10^{-5}$ μJy, which agrees well with the peak flare value measured by Fermi because converting it into microjanskys yields $F_{\rm SSC}^{Fermi} \sim 1.3\times10^{-5}$ μJy. Finally, to obtain an estimate of the order of magnitude of the associated uncertainties and given the non-linearity of Eqs. (1) and (2), we implemented a Markov chain Monte Carlo approach for S'_m, ν_m, and $\theta_{\rm mas}$. Specifically, for ν_m we chose a rather agnostic approach of assuming a uniform distribution between 20 GHz and 60 GHz, while for the other two parameters, normal distributions (with an uncertainty of $\delta\theta_{\rm mas} = [0.10, 0.4]$ mas, based on geometrical model-fitting; see Paraschos et al. 2024c; Kam et al. 2024, and $\delta S'_m = [1.1, 2.3]$ Jy, based on the spectrum with the α used in the calculations above). Our analysis resulted in [16th–84th] percentile limits of $\delta B_{\rm SSA} = [0.02, 61.33]$ G and $F_{\rm SSC} = [0, 380]\times10^{-5}$ μJy, emphasising the uncertainty of this

calculation. Expressed in terms of average and standard deviation, $B_{\rm SSA} = 10^{0.1\pm2.0}$ G and $F_{\rm SSC} = 10^{-5.4\pm3.5}$ μJy.

Second, we examined the behaviour of the VLBI EVPAs. In our case, they remained at a consistent orientation perpendicular to the bulk jet flow in the core region, but were variable close to the C3 region. At the December 15, 2024, epoch (see Fig. 2), the EVPAs in the C3 region appeared to follow the jet direction locally, similar to the results for the X-rays. Their variability, however, in the adjacent epochs indicates towards turbulence, which could be the mechanism that correlates the increase in the radio linear polarisation with the γ-ray emission. Thus, taking our twofold approach into account in combination with the insights of the accompanying X-ray analysis, we find that synchrotron self-Compton emission is indeed a viable mechanism.

4. Conclusions

We presented VLBI observations of 3C 84 taken during a γ-ray flare. We performed a study to localise the origin of these γ-ray photons via polarimetric imaging of the VLBI epochs. Our findings are summarised below.

- The analysis of centimetre and millimetre VLBI epochs of 3C 84 before, during, and after a γ-ray flare revealed increased linearly polarised emission at ∼1.5 parsec downstream of the central engine.
- Simultaneously taken X-ray measurements show a clear detection of polarised X-ray emission in the source, which, in combination with the radio data discussed here, provides a circumstantial indication that the blazar zone is beyond the ultimate vicinity of the central engine, and the up-scattering mechanism might be synchrotron self-Compton emission.

In summary, our results support a far-site scenario in which γ-rays are produced beyond the broad-line region of 3C 84. However, our work does not exclude that the near-site scenario also plays a role during other periods of intense activity within the jet.

Data availability

The polarised images presented in this work are available at the CDS via https://cdsarc.cds.unistra.fr/viz-bin/cat/J/A+A/709/A92

Acknowledgements. We thank the anonymous referee for their valuable comments which greatly improved this manuscript. We thank Dan Homan for performing part of the MOJAVE data analysis used in this work. This research is supported by the European Research Council advanced grant "M2FINDERS – Mapping Magnetic Fields with INterferometry Down to Event hoRizon Scales" (Grant No. 101018682). I. Liodakis was funded by the European Union ERC-2022-STG – BOOTES – 101076343. Views and opinions expressed are however those of the author(s) only and do not necessarily reflect those of the European Union or the European Research Council Executive Agency. Neither the European Union nor the granting authority can be held responsible for them. Y. Y. Kovalev was supported by the MuSES project, which has received funding from the European Union (ERC grant agreement No 101142396). Views and opinions expressed are however those of the author(s) only and do not necessarily reflect those of the European Union or ERCEA. Neither the European Union nor the granting authority can be held responsible for them. A. B. Pushkarev is supported in the framework of the State project 'Science' by the Ministry of Science and Higher Education of the Russian Federation under the contract 075-15-2024-541. C. Casadio and D. Álvarez-Ortega acknowledge support from the European Research Council (ERC) under the Horizon ERC Grants 2021 programme under grant agreement No.101040021. The University of New Hampshire group is supported in part by NASA Astrophysics Astrophysics Data Analysis Program grant 80NSSC24K0636. The POLAMI observations reported here were carried out at the IRAM 30 m Telescope. IRAM is supported by INSU/CNRS (France), MPG (Germany) and IGN (Spain). The Submillimeter Array (SMA) is a joint project between the Smithsonian Astrophysical Observatory and the Academia Sinica Institute of Astronomy and Astrophysics and is funded by the Smithsonian Institution and the Academia Sinica. Maunakea, the location of the SMA, is a culturally important site for the indigenous Hawaiian people; we are privileged to study the cosmos from its summit. The KVN is a facility operated by the Korea Astronomy and Space Science Institute. The KVN operations are supported by KREONET (Korea Research Environment Open NETwork) which is managed and operated by KISTI (Korea Institute of Science and Technology Information). S. Kang, S.-S. Lee, W. Y. Cheong, S.-H. Kim, and H.-W. Jeong were supported by the National Research Foundation of Korea (NRF) grant funded by the Korea government (MIST) (2020R1A2C2009003, RS-2025-00562700). The IAA-CSIC co-authors acknowledge financial support from the Spanish "Ministerio de Ciencia e Innovación" (MCIN/AEI/ 10.13039/501100011033) through the Center of Excellence Severo Ochoa award for the Instituto de Astrofísica de Andalucía-CSIC (CEX2021-001131-S), and through grants PID2019-107847RB-C44 and PID2022-139117NB-C44. This study makes use of VLBA data from the VLBA-BU Blazar Monitoring Program (BEAM-ME and VLBA-BU-BLAZAR; http://www.bu.edu/blazars/BEAM-ME.html), funded by NASA through the Fermi Guest Investigator Program. The VLBA is an instrument of the National Radio Astronomy Observatory. The National Radio Astronomy Observatory is a facility of the National Science Foundation operated by Associated Universities, Inc. This research has made use of data from the MOJAVE database that is maintained by the MOJAVE team (Lister et al. 2018). This research has made use of the NASA/IPAC Extragalactic Database (NED), which is operated by the Jet Propulsion Laboratory, California Institute of Technology, under contract with the National Aeronautics and Space Administration. This research has also made use of NASA's Astrophysics Data System Bibliographic Services. Finally, this research made use of the following python packages: *numpy* (Harris et al. 2020), *scipy* (Virtanen et al. 2020), *matplotlib* (Hunter 2007), *astropy* (Astropy Collaboration 2013, 2018) and *Uncertainties: a Python package for calculations with uncertainties.*

References

Abdo, A. A., Ackermann, M., Ajello, M., et al. 2009, ApJ, 699, 31
Abdollahi, S., Ajello, M., Baldini, L., et al. 2023, ApJS, 265, 31
Agudo, I., Jorstad, S. G., Marscher, A. P., et al. 2011, ApJ, 726, L13
Agudo, I., Thum, C., Molina, S. N., et al. 2018, MNRAS, 474, 1427
Astropy Collaboration (Robitaille, T. P., et al.) 2013, A&A, 558, A33
Astropy Collaboration (Price-Whelan, A. M., et al.) 2018, AJ, 156, 123
Backer, D. C., Wright, M. C. H., Plambeck, R. L., et al. 1987, ApJ, 322, 74
Benke, P., Savolainen, T., & Giovannini, G. 2026, A&A, in press, https://doi.org/10.1051/0004-6361/202553859
Biteau, J., & Giebels, B. 2012, A&A, 548, A123
Blandford, R. D., & Levinson, A. 1995, ApJ, 441, 79
Chael, A. A., Johnson, M. D., Narayan, R., et al. 2016, ApJ, 829, 11
Chael, A. A., Johnson, M. D., Bouman, K. L., et al. 2018, ApJ, 857, 23
Clausen-Brown, E., & Lyutikov, M. 2012, MNRAS, 426, 1374
Dotson, A., Georganopoulos, M., Meyer, E. T., & McCann, K. 2015, ApJ, 809, 164
Event Horizon Telescope Collaboration (Akiyama, K., et al.) 2019, ApJ, 875, L1
Event Horizon Telescope Collaboration (Akiyama, K., et al.) 2021, ApJ, 910, L12
Event Horizon Telescope Collaboration (Akiyama, K., et al.) 2022, ApJ, 930, L12
Fromm, C. M., Perucho, M., Mimica, P., & Ros, E. 2016, A&A, 588, A101
Fuhrmann, L., Angelakis, E., Zensus, J. A., et al. 2016, A&A, 596, A45
Giannios, D., Uzdensky, D. A., & Begelman, M. C. 2009, MNRAS, 395, L29
Giovannini, G., Savolainen, T., Orienti, M., et al. 2018, Nat. Astron., 2, 472
Harris, C. R., Millman, K. J., van der Walt, S. J., et al. 2020, Nature, 585, 357
Hodgson, J. A., Rani, B., Lee, S.-S., et al. 2018, MNRAS, 475, 368
Hodgson, J. A., Rani, B., Oh, J., et al. 2021, ApJ, 914, 43
Holdaway, M. A., & Wardle, J. F. C. 1990, ApJ, 349, 675
Homan, D. C., & Wardle, J. F. C. 2004, ApJ, 602, L13
Hovatta, T., & Lindfors, E. 2019, New Astron. Rev., 87, 101541
Hughes, P. A., Aller, M. F., & Aller, H. D. 2011, ApJ, 735, 81
Hunter, J. D. 2007, Comput. Sci. Eng., 9, 90
Janssen, M., Falcke, H., Kadler, M., et al. 2021, Nat. Astron., 5, 1017
Jorstad, S., & Marscher, A. 2016, Galaxies, 4, 47
Jorstad, S. G., Marscher, A. P., Smith, P. S., et al. 2013, ApJ, 773, 147
Jorstad, S. G., Marscher, A. P., Morozova, D. A., et al. 2017, ApJ, 846, 98
Kam, M., Hodgson, J. A., Park, J., et al. 2024, ApJ, 970, 176
Kang, S., Lee, S.-S., & Byun, D.-Y. 2015, J. Korean Astron. Soc., 48, 257
Kim, J. Y., Krichbaum, T. P., Marscher, A. P., et al. 2019, A&A, 622, A196
Kramarenko, I. G., Pushkarev, A. B., Kovalev, Y. Y., et al. 2022, MNRAS, 510, 469
Kramer, J. A., MacDonald, N. R., Paraschos, G. F., & Ricci, L. 2024, A&A, 691, A14

Krichbaum, T. P., Witzel, A., Graham, D. A., et al. 1992, A&A, 260, 33
Lähteenmäki, A., & Valtaoja, E. 2003, ApJ, 590, 95
Lico, R., Giroletti, M., Orienti, M., et al. 2017, A&A, 606, A138
Lindfors, E. J., Türler, M., Valtaoja, E., et al. 2006, A&A, 456, 895
Liodakis, I., Blinov, D., Jorstad, S. G., et al. 2020, ApJ, 902, 61
Liodakis, I., Chakraborty, S., Marin, F., et al. 2025, ApJ, 994, L9
Lister, M. L., Aller, M. F., Aller, H. D., et al. 2018, ApJS, 234, 12
Lister, M. L., Homan, D. C., Hovatta, T., et al. 2019, ApJ, 874, 43
MacDonald, N. R., & Nishikawa, K. I. 2021, A&A, 653, A10
MacDonald, N. R., Jorstad, S. G., & Marscher, A. P. 2017, ApJ, 850, 87
Marin, F., Pursimo, T., Liodakis, I., et al. 2025, A&A, 702, L16
Marscher, A. P. 1983, ApJ, 264, 296
Marscher, A. P., Jorstad, S. G., Agudo, I., MacDonald, N. R., & Scott, T. L. 2012, ArXiv e-prints [arXiv:1204.6707]
Monti-Guarnieri, P., & Bernard, D. 2025, ATel, 16988, 1
Nagai, H., Suzuki, K., Asada, K., et al. 2010, PASJ, 62, L11
Nagai, H., Haga, T., Giovannini, G., et al. 2014, ApJ, 785, 53
Nagai, H., Fujita, Y., Nakamura, M., et al. 2017, ApJ, 849, 52
Narayan, R., & Piran, T. 2012, MNRAS, 420, 604
Paraschos, G. F. 2025, A&A, 695, L3
Paraschos, G. F., & Mpisketzis, V. 2025, A&A, 696, L7
Paraschos, G. F., Kim, J. Y., Krichbaum, T. P., & Zensus, J. A. 2021, A&A, 650, L18
Paraschos, G. F., Krichbaum, T. P., Kim, J. Y., et al. 2022, A&A, 665, A1
Paraschos, G. F., Mpisketzis, V., Kim, J. Y., et al. 2023, A&A, 669, A32
Paraschos, G. F., Debbrecht, L. C., Kramer, J. A., et al. 2024a, A&A, 686, L5
Paraschos, G. F., Kim, J. Y., Wielgus, M., et al. 2024b, A&A, 682, L3
Paraschos, G. F., Wielgus, M., Benke, P., et al. 2024c, A&A, 687, L6
Paraschos, G. F., Traianou, E., Debbrecht, L. C., Liodakis, I., & Ros, E. 2025, ApJ, 989, 208
Park, J., Kino, M., Nagai, H., et al. 2024, A&A, 685, A115
Planck Collaboration XIII. 2016, A&A, 594, A13
Pushkarev, A. B., Butuzova, M. S., Kovalev, Y. Y., & Hovatta, T. 2019, MNRAS, 482, 2336
Rani, B., Krichbaum, T. P., Lee, S. S., et al. 2017, MNRAS, 464, 418
Savolainen, T., Giovannini, G., Kovalev, Y. Y., et al. 2023, A&A, 676, A114
Sikora, M., Begelman, M. C., & Rees, M. J. 1994, ApJ, 421, 153
Sinitsyna, V. G., & Sinitsyna, V. Y. 2025, ApJ, 985, 39
Soffitta, P., Baldini, L., Baumgartner, W., et al. 2023, SPIE Conf. Ser., 12678, 1267803
Strauss, M. A., Huchra, J. P., Davis, M., et al. 1992, ApJS, 83, 29
Traianou, E., Gómez, J. L., Cho, I., et al. 2025, A&A, 700, A16
Traianou, E., Bruni, G., & Rodi, J. 2026, A&A
Valtaoja, E., Terasranta, H., Urpo, S., et al. 1992, A&A, 254, 71
Virtanen, P., Gommers, R., Oliphant, T. E., et al. 2020, Nat. Methods, 17, 261
Weaver, Z. R., Jorstad, S. G., Marscher, A. P., et al. 2022, ApJS, 260, 12
Weisskopf, M. C., Soffitta, P., Baldini, L., et al. 2022, J. Astron. Telesc. Instrum. Syst., 8, 026002

[1] Finnish Centre for Astronomy with ESO, University of Turku, 20014 Turku, Finland
[2] Aalto University Metsähovi Radio Observatory, Metsähovintie 114, FI-02540 Kylmälä, Finland
[3] Max-Planck-Institut für Radioastronomie, Auf dem Hügel 69, D-53121 Bonn, Germany
[4] Institute of Astrophysics, Foundation for Research and Technology – Hellas, Voutes 7110, Heraklion, Greece
[5] Institute for Astrophysical Research, Boston University, 725 Commonwealth Avenue, Boston, MA 02215, USA
[6] Saint Petersburg State University, 7/9 Universitetskaya nab., St. Petersburg 199034, Russia
[7] NASA Marshall Space Flight Center, Huntsville, AL 35812, USA
[8] Université de Strasbourg, CNRS, Observatoire Astronomique de Strasbourg, UMR 7550, 67000 Strasbourg, France
[9] Interdisziplinäres Zentrum für wissenschaftliches Rechnen (IWR), Ruprecht-Karls-Universität Heidelberg, Im Neuenheimer Feld 205, 69120 Heidelberg, Germany
[10] Instituto de Astrofísica de Andalucía, IAA-CSIC, Glorieta de la Astronomía s/n, E-18008 Granada, Spain
[11] Department of Physics and Astronomy and Space Science Center, University of New Hampshire, Durham, NH 03824, USA
[12] ASI – Agenzia Spaziale Italiana, Via del Politecnico snc, 00133 Roma, Italy
[13] INAF, Istituto di Astrofisica e Planetologia Spaziali, Via Fosso del Cavaliere 100, 00133 Roma, Italy
[14] Physical Research Laboratory, Thaltej, Ahmedabad, Gujarat 380009, India
[15] Science & Technology Institute, Universities Space Research Association, 320 Sparkman Drive, Huntsville, AL 35805, USA
[16] Dipartimento di Fisica, Universitá degli Studi di Roma "Tor Vergata", Via della Ricerca Scientifica 1, 00133 Roma, Italy
[17] Istituto Nazionale di Fisica Nucleare, Sezione di Roma "Tor Vergata", Via della Ricerca Scientifica 1, 00133, Roma, Italy
[18] Crimean Astrophysical Observatory, 298409 Nauchny, Crimea
[19] Institute for Nuclear Research of the Russian Academy of Sciences, 60th October Anniversary Prospect 7a, Moscow 117312, Russia
[20] Lebedev Physical Institute, Pushchino Radio Astronomy Observatory, Radiotelescopnaya 1a, Pushchino 142290, Russia
[21] Aalto University Department of Electronics and Nanoengineering, PL 15500, FI-00076 Aalto, Finland
[22] Institut de Radioastronomie Millimétrique, Avenida Divina Pastora, 7, Local 20, E–18012 Granada, Spain
[23] Center for Astrophysics | Harvard & Smithsonian, 60 Garden Street, Cambridge, MA 02138, USA
[24] Korea Astronomy and Space Science Institute, 776 Daedeok-daero, Yuseong-gu, Daejeon 34055, Korea
[25] University of Science and Technology, Korea, 217 Gajeong-ro, Yuseong-gu, Daejeon 34113, Korea
[26] Department of Physics, University of Crete, 70013 Heraklion, Greece
[27] Max Planck Institute for Astrophysics, Karl-Schwarzschild-Str. 1, D-85741 Garching, Germany
[28] INAF, Istituto di Astrofisica Spaziale e Fisica Cosmica di Milano, Via Alfonso Corti 12, I – 20133 Milano, Italy
[29] Universitäts-Sternwarte, Fakultät für Physik, Ludwig-Maximilians-Universität München, Scheinerstr.1, 81679 München, Germany
[30] INFN, Sezione di Pavia, Via A. Bassi 6, 27100 Pavia, Italy
[31] INAF Osservatorio Astronomico di Brera, Via E. Bianchi 46, 23807 Merate, (LC), Italy
[32] Department of Astronomy and Astrophysics, The University of Chicago, Chicago, IL 60637, USA

Appendix A: CLEAN reconstruction of 43 GHz data

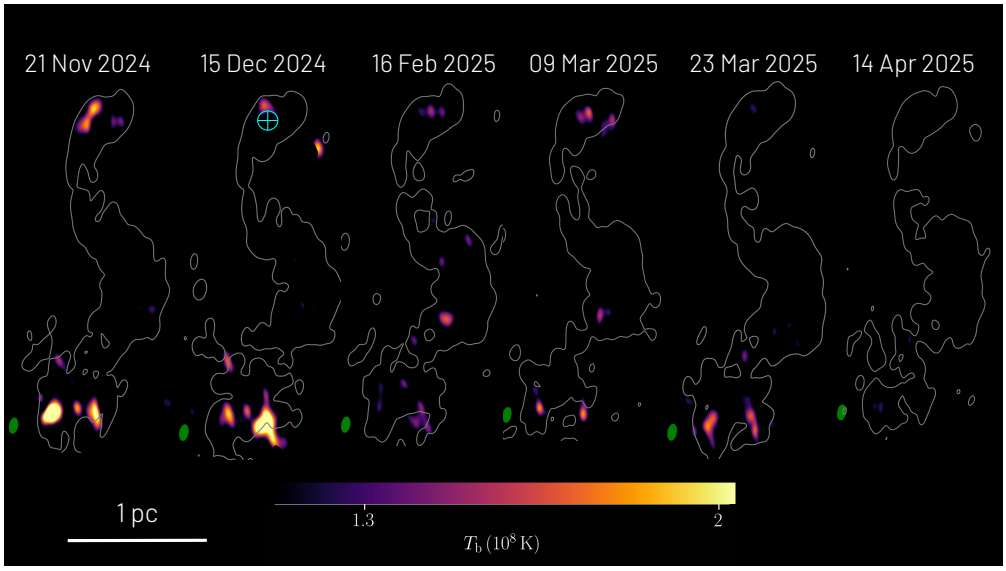

Fig. A.1. Publicly available CLEAN-reconstruction images of 3C 84 at 43 GHz (BEAM-ME). The display is in a similar manner to the bottom panel of Fig. 2. The green ellipse next to each reconstruction illustrates the restoring CLEAN-beam, which corresponds to (0.15×0.30) mas $(10°)$ on average. We note the consistency between the RML and CLEAN reconstructions. Specifically, the core region of 3C 84 exhibits a lower linear polarisation signal, whereas the C3 region appears brighter in the November and December 2024 epochs (around the time of the flare) before also returning to a lower signal state.

Appendix B: Total intensity flux density light curve

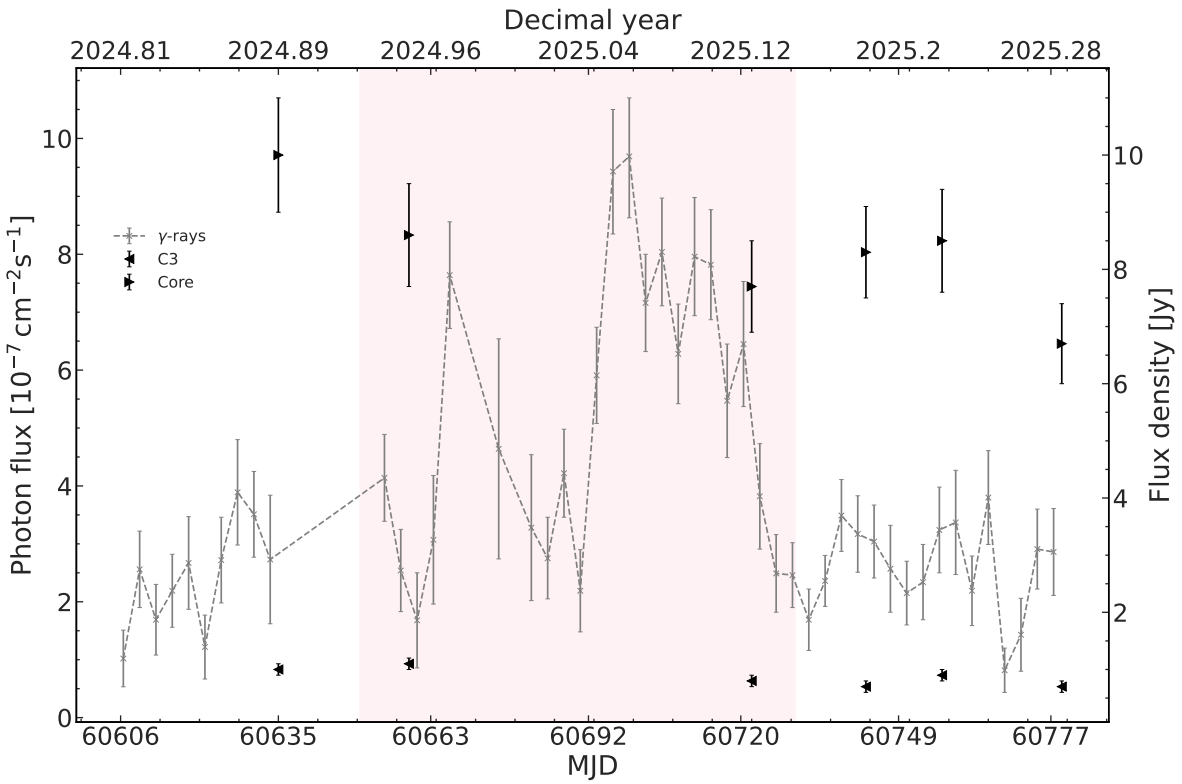

Fig. B.1. Total intensity flux density light curve of the core and C3 region, displayed along the γ-ray light curve. The setup of the figure is similar to Fig. 1. While the core flux density remains stable during the γ-ray flare, the one of the C3 region is higher, following the same trend as the polarisation degree.